Strong lensing of gamma ray bursts as a probe of compact dark matter

Lingyuan Ji, Ely D. Kovetz, and Marc Kamionkowski

Strong Lensing of Gamma Ray Bursts as a Probe of Compact Dark Matter

Lingyuan Ji,[1] Ely D. Kovetz,[1] and Marc Kamionkowski[1]

[1]*Department of Physics and Astronomy, Johns Hopkins University,*
3400 N. Charles St., Baltimore, MD 21218, USA

Compact dark matter has been efficiently constrained in the $M \lesssim 10\,M_\odot$ mass range by null searches for microlensing of stars in nearby galaxies. Here we propose to probe the mass range $M \gtrsim 10\,M_\odot$ by seeking echoes in gamma-ray-burst light curves induced by strong lensing. We show that strong gravitational lensing of gamma ray bursts (GRBs) by massive compact halo objects (MACHOs) generates superimposed GRB images with a characteristic time delay of $\gtrsim 1\,\mathrm{ms}$ for $M \gtrsim 10\,M_\odot$. Using dedicated simulations to capture the relevant phenomenology of the GRB prompt emission, we calculate the signal-to-noise ratio required to detect GRB lensing events as a function of the flux ratio and time delay between the lensed images. We then analyze existing data from the Fermi/GBM and Swift/BAT instruments to assess their constraining power on the compact dark matter fraction f_{DM}. We find that this data is noise limited, and therefore localization-based masking of background photons is a key ingredient. Future observatories with better sensitivity will be able to probe down to the $f_{\mathrm{DM}} \gtrsim 1\%$ level across the $10\,M_\odot \lesssim M \lesssim 1000\,M_\odot$ mass range.

I. INTRODUCTION

While various independent experiments have garnered evidence for the existence of dark matter for nearly 50 years, what constitutes it remains a mystery [1]. An important class of candidates to make up the dark matter are massive compact halo objects (MACHOs) [2]. The MACHO scenario is well constrained at the low mass range ($\lesssim 10 M_\odot$) by the fact that we only observe a small optical depth of gravitational microlensing for stars in nearby galaxies [3, 4]. Meanwhile, the higher mass range ($\gtrsim 100 M_\odot$) is constrained by various dynamical considerations (such as perturbing effects from MACHOs on Galactic wide binaries [5–7] or the compactness of star clusters and ultra-faint dwarf galaxies [8]), and by lack of radiation as a result of accretion from the CMB (if the compact dark matter are primordial black holes) [9–12].

The intermediate mass range, $10 M_\odot \lesssim M_L \lesssim 100 M_\odot$, has received a lot of attention following the recent LIGO detection of several merging black hole binaries [13] and the suggestion that these may be primordial black holes (PBHs) [14, 15] which could comprise a significant fraction of the total dark matter in the Universe [16–19]. This mass range remains less robustly constrained [20], and novel approaches to probing it are well motivated [21].

In this paper we propose to seek MACHOs in the $\gtrsim 10\,M_\odot$ mass range by searching gamma-ray-burst (GRB) light curves for signs of microlensing induced echoes. GRBs are extremely energetic explosions originating in distant galaxies that lead to rapid emission of high-energy gamma rays [22–24]. Several thousands of GRBs have been detected to date by dedicated instruments such as BATSE, FERMI GBM and SWIFT BAT. The prompt emissions of observed GRBs last from $\sim 10\,\mathrm{ms}$ to $\sim$ hours and the source redshifts are $\mathcal{O}(z = 1)$.

Strong lensing by a massive compact lens will generate two images of the original GRB [25, 26]. The angular separation between the images is too small to be probed by current observations [27–29]. But the arrival times of the two images differ by roughly the Schwarzchild crossing time, roughly $0.3\,(M_L/10\,M_\odot)$ milliseconds for a lens of mass M_L. Here we build upon Ref. [30], wherein it was suggested that these microlensing-induced echoes can be sought with fast radio bursts (FRBs), to explore the possibility to seek these echoes with GRBs. Unlike Fast Radio Bursts (FRBs) [30], whose intrinsic time width is short ($\sim 1\,\mathrm{ms}$), the images of strongly lensed GRBs will not appear as separate consecutive bursts. Rather, the fluxes from the two images will be added up to give the total light curve measured by a GRB observatory. However, lensed GRBs with time delays longer than the minimum variability timescale (MVT) of the intrinsic burst signal could be resolved by the correlation between the displaced features in the overlaid first and second images, which will generate a peak in autocorrelation of the total light curve. As we show below, with MVT $\sim 1\,\mathrm{ms}$ [31], it is possible to probe MACHO lens masses $M_L \gtrsim 10 M_\odot$.

Although detecting repeating FRBs is simpler due to their cleaner temporal shape, GRBs are detectable out to higher redshifts. As a result, for the same MACHO mass M_L and fraction f_{DM} of the total dark matter that is made up of MACHOs, the integrated lensing optical depth becomes larger, which increases the sensitivity of our probe. Furthermore, a higher lens redshift will yield a longer time delay, which extends the mass range we can probe at the lower end, given the same MVT.

The idea to seek lensing-induced GRB echoes traces back to Ref. [32], and there have been searches for GRB repeaters [33–36]. Refs. [37–41] studied repeated bursts induced by lensing. Ref. [40] looked for similarities in light-curve shapes between different bursts. Ref. [41] used a similar auto-correlation method as we do here to seek echoes within individual light curves. We extend upon this method by performing new simulation tests, including updated datasets, and focusing more on the push to shorter-timescale echoes, as we search for lensing induced by dark-matter lenses rather than Pop III stars.

In Section II, we review the theory of strong gravitational lensing by a point mass lens and the calcula-

tion of the lensing optical depth. In Section III, we introduce an algorithm to detect strongly lensed GRB. In Section IV, we reduce the Fermi Gamma-ray Burst Monitor (Fermi/GBM) and Swift Burst Alert Telescope (Swift/BAT) TTE data and show how to determine the detection cross Section from the data, based on a comparison with dedicated simulations we develop for this purpose. In Section IV C, we show the best constraints we can reach for various cases considered. We discuss future improvements in V and conclude in Section VI.

II. THEORY

A MACHO of mass M_L can be modeled as a point mass lens [25, 26] with an angular Einstein radius

$$\theta_E = 2\sqrt{\frac{GM_L}{c^2}\frac{D_{LS}}{D_S D_L}}, \tag{1}$$

where D_S, D_L and D_{LS} are the angular diameter distances from the observer to the source, to the lens and between the source and lens, respectively. The two images produced by the gravitational lensing lie at angular positions

$$\theta_\pm = \frac{\beta \pm \sqrt{\beta^2 + 4\theta_E^2}}{2}, \tag{2}$$

where β is the angular impact parameter. The time delay between these two images can be shown to be [30]

$$\Delta t = \frac{4GM_L}{c^3}(1+z_L)\left[\frac{y}{2}\sqrt{y^2+4} + \ln\left(\frac{\sqrt{y^2+4}+y}{\sqrt{y^2+4}-y}\right)\right], \tag{3}$$

where $y \equiv \beta/\theta_E$ is the impact parameter normalized by the Einstein radius and z_L is the lens redshift. The difference in luminosity between these two images can be characterized by a flux ratio R defined as

$$R \equiv \left|\frac{\mu_+}{\mu_-}\right| = \frac{(y^2+2)+y\sqrt{y^2+4}}{(y^2+2)-y\sqrt{y^2+4}}, \tag{4}$$

where μ_+ and μ_- are the magnifications of the two images, respectively. Note that for a given lens mass M_L and lens redshift z_L, both R and Δt as a function of y are monotonic.

If the lensing-induced echo is to be detectable, the impact parameter must satisfy two conditions. First, there exists a minimum detectable time delay $\overline{\Delta t}$, where for any $\Delta t < \overline{\Delta t}$ the time delay between the images is too short to be resolved by autocorrelation method. Secondly, there exists a maximum detectable magnification ratio $\overline{R}$, where for any $R > \overline{R}$ the second image is too weak to be detected. Therefore, the impact parameter y is bounded at the lower end by the minimum permitted time delay $\overline{\Delta t}$, as well as at the higher end by the

maximum allowed magnification $\overline{R}$. This determines an effective cross section,

$$\sigma(M_L, z_L, z_S; \overline{R}, \overline{\Delta t}) = \pi\theta_E^2 \text{Ramp}[y_{\max}^2(\overline{R}) - y_{\min}^2(M_L, z_L, \overline{\Delta t})], \tag{5}$$

for a single lens given by an annulus between the maximum and minimum impact parameters. The cross section we defined here is not the same as the conventional one defined in particle physics. We define it to be the solid angle spanned by the annulus. It is hence dimensionless. In Eq. 5, $\text{Ramp}(x) = (x + |x|)/2$ is the ramp function. Note that the implicit z_S dependence emerges through the angular diameter distances D_{LS}, D_S in θ_E [42].

To find the optical depth of a GRB at redshift z_S to be lensed by a MACHO on its way to Earth, in the optically-thin regime, we need to integrate over the cross sections. In our model we take all MACHOs to be of the same mass and uniformly distributed in the Universe. This gives

$$\tau(z_S, M_L, f_{\text{DM}}; \overline{R}, \overline{\Delta t}) = \int_0^{z_S} d\chi(z_L)\,(1+z_L)^2 n_L \\ \times \sigma(M_L, z_L, z_S; \overline{R}, \overline{\Delta t}) \tag{6}$$

where $\chi(z)$ is the comoving distance as a function of redshift z, $d\chi(z_L) = c\,dz_L/H(z_L)$, where $H(z_L)$ is the Hubble parameter at redshift z_L, and n_L is the MACHO comoving number density (which can be related to f_{DM} by $f_{\text{DM}} = 8\pi G n_L M_L c^2/3H_0^2\Omega_d$). Using the GRB redshift distribution $N(z_S)$ [43, 44], the total optical depth is

$$\tau_{\text{tot}}(M_L, f_{\text{DM}}; \overline{R}, \overline{\Delta t}) = \int N(z_S)dz_S\,\tau(z_S, M_L, f_{\text{DM}}; \overline{R}, \overline{\Delta t}). \tag{7}$$

If in a catalog containing N GRBs, a certain algorithm can pick out no more than N_* events as lensed, up to a specific cross section criterion $(\overline{R}, \overline{\Delta t})$, then $\tau_{\text{tot}} < N_*/N$ can be put as a constraint. As an example, we plot in Fig. 1 the constraints to the f_{DM}-M_L parameter space that would arise from a null search in a dataset of size $N \sim 2000$. Here some representative values of $\overline{\Delta t}$ and $\overline{R}$ are chosen. Comparing to the FRB case [30], where the integrated optical depth is $\tau_{\text{tot}} \sim 2\%$ (for $\overline{R} = 5.0$ and $f_{\text{DM}} = 1$) within the sensitive mass range, for GRBs it increases to $\tau_{\text{tot}} \sim 15\%$ under the same conditions (and reduces to $\tau_{\text{tot}} \sim 6\%$ for $\overline{R} = 3.0$).

In principle, the limitation on Δt comes from the MVT of the light curve, while the limitation on R is mainly related to the light curve's signal-to-noise ratio (SNR). The specific algorithm one uses to detect the lensing feature in the light curves will affect these two limitations as well.
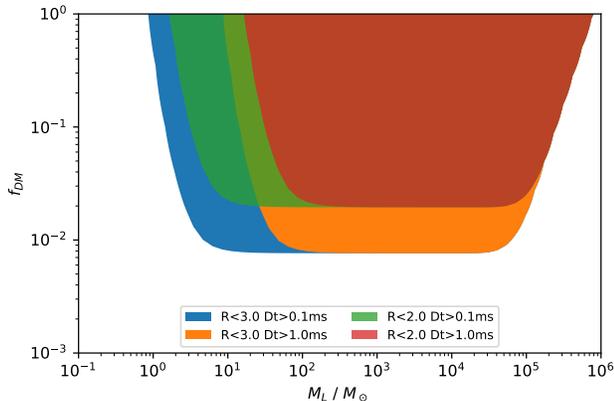
FIG. 1. Fraction $f_{\rm DM}$ of dark matter than can be probed for different lens masses M_L in a dataset of size $N \sim 2000$. Each patch is calculated with different minimum detectable time delay cutoff $\overline{\Delta t}$ and maximum detectable magnification ratio cutoff $\overline{R}$. In each case, the sensitivity is reduced at the low mass end because the generated time delay is too small to resolve; at the high mass range, the sensitivity is reduced because, practically, the detectable time delay will also have an upper bound due to the maximum correlation time probed. Here we take it to be 3 secs.

III. METHOD

A. Light Curve Autocorrelation

In the case of FRBs [30]—which are intrinsically very short ($\sim 1\,\mathrm{ms}$)—a lensed burst would appear as two distinct peaks, whose time delay can then be read manifestly, provided that the flux ratio is not too small. GRBs, however, are a different story, as their duration can range from milliseconds to minutes (and longer). The light curve of a a strongly lensed GRB will have an echo superimposed on the light curve. To detect this, we define the autocorrelation function,

$$C(\delta t) \equiv \frac{\int dt\, I(t)I(t-\delta t)}{\sqrt{\int dt\, I^2(t)}\sqrt{\int dt\, I^2(t-\delta t)}}, \qquad (8)$$

of a light curve $I(t)$ [41, 45]. This is the normalized cross correlation between a function and its shifted self. Note that $C(0) = 1$. For generic non-autocorrelated functions, $C(\delta t \neq 0) < 1$, and thus $\delta t = 0$ serves as the only major spike in the function $C(\delta t)$.

The effectiveness of the autocorrelation analysis on strongly lensed data can be shown as follows. Let $I(t)$ be the intrinsic light curve of the GRB event and $C(\delta t)$ its autocorrelation. In a specific lensing configuration, Eqs. (3) and (4) assign a time delay Δt and a flux ratio R to the second image, yielding a lensed light curve

$$I(t; \Delta t, R) \propto \frac{R}{R+1}I(t) + \frac{1}{R+1}I(t-\Delta t). \qquad (9)$$

It is easy to see that the autocorrelation of the lensed light curve $I(t; \Delta t, R)$ is then given by

$$\begin{aligned}
&C(\delta t; \Delta t, R) \\
&= \frac{(R^2+1)C(\delta t) + R[C(\delta t + \Delta t) + C(\delta t - \Delta t)]}{(R^2+1) + 2RC(\Delta t)}.
\end{aligned} \qquad (10)$$

According to this formula, the lensed signal will exhibit spikes at $\delta t = -\Delta t, 0, +\Delta t$ with an amplitude ratio $R/(R^2+1) : 1 : R/(R^2+1)$.

B. Detection Algorithm

Real data, however, result in a spiky structure even for $C(\delta t)$, which means $\delta t = -\Delta t, 0, +\Delta t$ are not the only spikes in $C(\delta t; \Delta t, R)$. To distinguish lensing-induced spikes from noise, we define the sigma parameter

$$\sigma = \sqrt{\frac{\sum_{\delta t \in D}[C(\delta t) - G(\delta t)]^2}{|D|}}, \qquad (11)$$

where $C(\delta t)$ is the autocorrelation one wants to check (can be lensed or not), $G(\delta t)$ is a Gaussian smoothing of $C(\delta t)$ and D is the time grid over which the calculation is performed. The radius of such Gaussian smoothing should be chosen to smooth out the lensing spikes. As we will argue in Section III C, the width of such spikes will be $\sim$ MVT. So, in Fig. 7 we take it to be the same as MVT = 1ms. The sigma parameter quantifies the overall spikiness in $C(\delta t)$ compared to a smooth template $G(\delta t)$. If we identify a δt for which $|G(\delta t) - C(\delta t)|$ is larger than some threshold (e.g. 3σ or 4σ), we can claim evidence for a spike due to lensing. In Fig. 2 we present the autocorrelations of a simulated unlensed/lensed GRB light curve. The simulation method is described in Section IV.

C. Noise and Minimum Variability Timescales

The two major reasons responsible for the limitations $\Delta t > \overline{\Delta t}$ and $R < \overline{R}$ in the gravitational lensing model are: (1) the amount of noise in the observed light curve; and (2) the minimum variability timescale. Eq. (10), the formulation of the autocorrelation of the lensed light curve, may help to show this. On the one hand, for the peaks at Δt to be separable from the peak at 0, the full width at half maximum (FWHM) should be smaller than Δt. However, the FWHM of an autocorrelation is approximately the signal's MVT. So we can take $\overline{\Delta t} \sim$ MVT. On the other hand, the amplitude $R/(R^2+1)$ of the peak at Δt has to compete with the amplitude of random peaks due to noise. This eventually sets $\overline{R}$.

It is worth stressing that there is a conceptual difference between this work and Ref. [30], which addressed strong lensing of FRBs by compact dark matter objects. There, the minimum detectable time delay was set by the temporal width of the FRB, which is typically $\mathcal{O}(1)\,\mathrm{ms}$.

autocorrelation: simulated, unlensed

autocorrelation: simulated, lensed
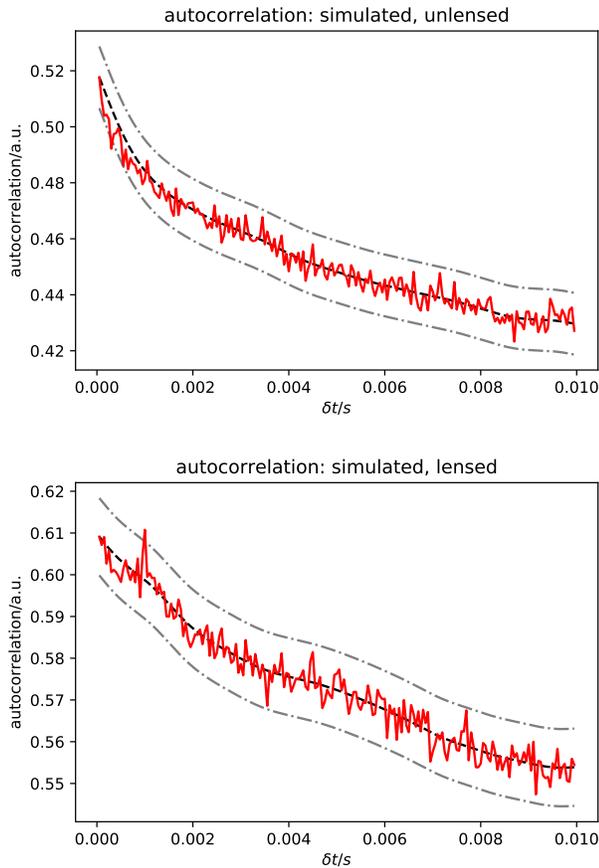
FIG. 2. Red line represents the light curve autocorrelation. Black dashed line is the Gaussian smoothing of autocorrelation. Gray dotted dashed lines are $\pm 3\sigma$. In the upper panel, no exceedance larger than 3σ is found, while in the lower panel there is an exceedance at $\delta t = 1$ms. It can be seen that this algorithm can effectively detect lensing events at a certain level. More discussion about the sensitivity of the algorithm can be found in Section IV and how to simulate the light curve is elaborated in Section IV.

Here, the temporal width of GRB is $T_{90} \sim$ seconds, which is much larger than the typical time delay for strong lensing by point source of $\gtrsim 10\,M_\odot$. The relevant question for determining the detectability of a lensed GRB through autocorrelation is what is the smallest timescale that still contains variability features that can autocorrelate. This shifts the limitation on the time delay to the MVT.

IV. APPLICATION

A. Overview of GRB observatories

From the previous Section, we see that the gravitational lensing time delay generated by $M_L \gtrsim 10\,M_\odot$ lenses requires a time resolution better than ~ 1ms. Fermi/GBM and Swift/BAT properly suit our purpose
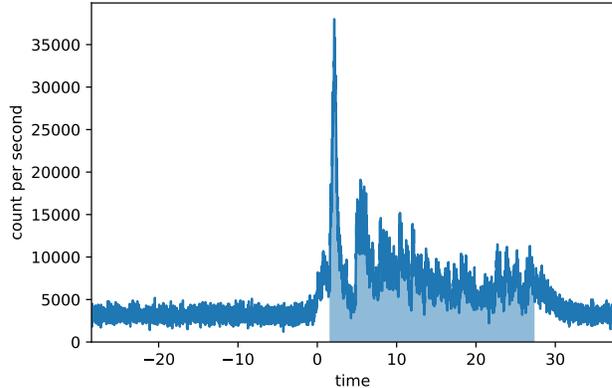
FIG. 3. `bn161218356` light curve (from Fermi/GBM). The trigger time is set to be the origin, while T_{90} range is shaded. The steady noise between $T_{90,\mathrm{start}} - 20$s and $T_{90,\mathrm{start}} - 10$s represents the noise. The T_{90} range represents the signal.

[27, 44]. If the experiment's trigger condition is reached, all detectors' TTE data will be recorded for the following several hundreds seconds, and a mask will be generated for triggered detectors. We use the this mask to sum up all the photons for the triggered detectors to get the array $\{t_i\}_{i=1}^n$. The data is then binned to generate a light curve. We use a subset of the Fermi/GBM catalog[1] with $N = 2274$ GRBs ($N = 1230$ for Swift/BAT[2]). An example light curve (trigger # `bn161218356`) is shown in Fig. 3.

B. Lensing Simulation

As presented in Section III A, a light curve model with the correct amount of noise added in is needed to obtain $\overline{R}$. Also, the MVT has to be incorporated in the model for us to verify the choice $\overline{\Delta t} = \mathrm{MVT}$. Here we employ a model where the observed lensed light curve is given by

$$
\begin{aligned}
&I(t; \Delta t, R; H, \mathrm{MVT}, A) \\
&= \frac{R}{1+R} B'_H(t) + \frac{1}{1+R} B'_H(t - \Delta t) + An(t),
\end{aligned}
\tag{12}
$$

where $B_H(t)$ is one realization of a fractional Brownian motion (fBm) [46] with Hurst index $H \in (0, 1)$, $B'_H(t)$ is $B_H(t)$ Gaussian filtered with radius $\mathrm{MVT}/2\pi$, $n(t)$ is a unit Gaussian noise (GN) and A quantifies the amplitude of noise in the measured light curve. We use fBm because it contains features on all timescales, which enables us to cut off the power spectrum at a chosen high frequency to simulate the MVT behavior. In addition, the power spectrum of fBm scales as $1/f^{2H+1}$ [47], which resembles

———
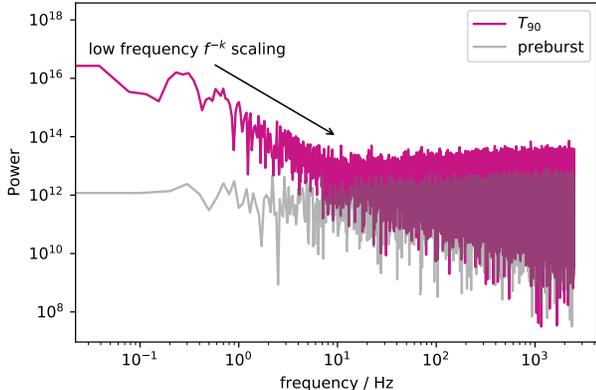
FIG. 4. The power spectrum of `bn161218356`. For the T_{90} range, a scaling feature $1/f^k$ can be seen at low frequency. In the pre-burst range, the power spectrum is scale independent, which is typical for gaussian noise.

FIG. 5. Effective Hurst index H_{eff} distribution for light curves in the Fermi/GBM catalog. The median of this distribution is approximately 0. Given that the allowed range for the Hurst index is $H \in (0, 1)$, we choose $H = 0.1$ in our simulations.

observed GRB light curves at low frequencies (Fig. 4). The value of H will be determined below using the data. The term $B'_H(t)$ corresponds to the image that arrives first and the term $B'_H(t - \Delta t)$ to the delayed image. The coefficients in front are the amplitudes of each image, chosen to produce the magnification ratio R while also maintaining the total signal strength the same as $B'_H(t)$.

In each lensing simulation, we fix the values of the parameters $\{H, \text{MVT}, A\}$ and sample the parameter space $(\Delta t, R)$. For each lensed light curve generated, the detection algorithm is applied to determine the significance of the lensing effect. A 3σ threshold is then used to set $\overline{\Delta t}$ and $\overline{R}$. To eliminate the bias from the specific profile of each specific light curve realization, the significance is averaged among an adequate amount of light curve realizations with the same set of chosen parameters.

To quantify the constraining power of Fermi/GBM or Swift/BAT, the parameters in our model, Eq. (12), need to be inferred from the data. We do this next.

C. Results

We first use the data to infer the suitable value of H. A fBm with Hurst index H will have a power spectrum scaling as $P \propto 1/f^{2H+1}$. The same scaling behavior exists in the Fermi/GBM and the Swift/BAT data; see for instance Fig. 4. We therefore fit the low frequency $(0 - 2 \text{ Hz})$ scaling part of the power spectrum using the template $P \propto 1/f^k$, and then set $H_{\text{eff}} \equiv (k - 1)/2$. The distribution of H_{eff} for the Fermi/GBM catalog is shown in Fig. 5. We see that the median value is $H_{\text{eff}} \approx 0.0$. Since the allowed range for H is $(0, 1)$, we fix $H = 0.1$.

The noise amplitude A is also related to the power spectrum. While the light curve signal has the scaling property above, Gaussian noise has equal power at all timescales. Therefore, the noise power will always be

dominant on the smallest time scales, as shown in Fig. 4. It is useful to define the ratio

$$r = \frac{P_{\text{median}}(T_{90} \text{ range, 0-2 Hz})}{P_{\text{median}}(\text{pre-burst, 10-30 Hz})} \quad (13)$$

of these two powers. On a specific grid the lensing simulation is performed, A can be expressed as a function of r. In our case, the simulation length is $1\,\text{s}$ with $t_{\text{bin}} = 50\,\mu\text{s}$. Numerical experiments show that a good approximation to take is

$$r \sim 1 + \frac{50\text{ms}}{t_{\text{bin}}} \frac{1}{A^2}. \quad (14)$$

The distributions of power ratio r in the Fermi/GBM and Swift/BAT datasets are shown in Fig. 6. A more detailed comparison is included in Appendix A. Note that only the value of r is physical, while A depends on the specific t_{bin} setup. We will solely refer to r for the simulations, keeping in mind that it is translated from Eq. (14).

With the scaling and noise parameters determined by observations, we proceed to test the detection algorithm. Here we choose MVT $= 100\mu$s, which will allow us to probe the interesting mass range $1M_\odot \lesssim M_L \lesssim 100M_\odot$. Larger MVTs could also be considered if needed. But the main effects of the instrumental sensitivity will be similar for any choice of MVT. The light curve simulation is performed on a $[0, 1]\,$s interval with $t_{\text{bin}} = 50\,\mu$s binning.

The results are shown in Fig. 7. We see that a 3σ (4σ) detection can be achieved with Fermi/GBM or Swift/BAT at $\overline{R} = 3.0$ (2.0), with MVT$=1\,\mu$ms and a light curve power ratio $r \sim 5000$. This ratio is much higher than the typical value for current data. This means that in order to use this method to detect lensed GRB, the noise amplitude (i.e. background photon counts) in a future GRB observatory would have to be decreased by a factor $\sqrt{5000/10} \sim 22$.
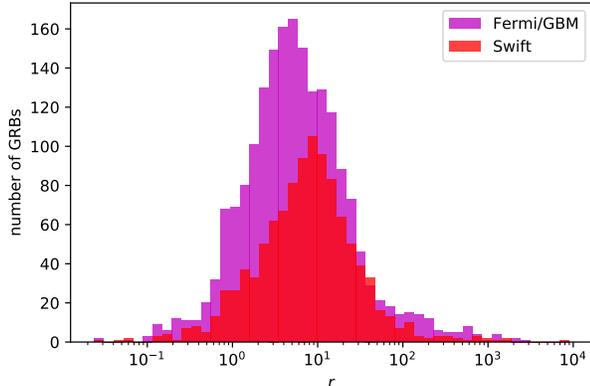
FIG. 6. Power ratio r distribution in Fermi/GBM and Swift/BAT. The number of GRBs with $r \geq 1000, 1500, 2000, 3000, 5000, 10000$ is $10, 4, 3, 1, 1, 0$ for GBM and $5, 3, 1, 1, 1, 0$ for BAT (using 1922 and 1060 GRBs from each catalog which have adequate data to calculate the power spectrum in this frequency range).

V. DISCUSSION

Evidently, a major restriction on the detectability of strongly lensed GRBs is the background photon noise. Typically, GRB observatories record photons with energy ranging from several keV to several hundreds of keV. In this range, photons from the cosmic X-ray background (CXB) and cosmic gamma-ray background (CGB) will act as noise, with CXB expected to be the dominant source. The rate of noise photons detected in Swift/BAT can be estimated by

$$
\text{rate} = \left(\frac{\int_{15\text{keV}}^{300\text{keV}} S_{\text{CXB}}(E) d \ln E}{2.33 \text{ events} \cdot \text{s}^{-1} \cdot \text{cm}^{-2} \cdot \text{sr}^{-1}} \right)
$$
$$
\times \left(\frac{\text{aperture}}{5200 \text{ cm}^2} \right) \left(\frac{\text{FOV}}{1.4 \text{ sr}} \right) 1.7 \times 10^4 \text{ events/sec},
$$
(15)

where $S_{\text{CXB}}(E)$ is the power spectrum of CXB, and $d \ln E$ counts the photon number. The integration is normalized to the value from Ref. [48], while the aperture size and the BAT field of view (FOV) are normalized as in Ref. [28]. Our estimate is consistent with that of Ref. [28]. It indicates that if one can effectively mask (background) photons originating from outside a region $\lesssim 1°$, based on the localization of the GRB, the signal-to-noise could be improved enough to enable the detection of strong lensing of GRBs by MACHOs in the $M_L \gtrsim 10 \, M_\odot$ range. Instruments using a coded-aperture mask may be able to achieve this (see discussion of BAT in the Appendix).

Another issue worth noting is that only a small fraction of GRBs have the required MVT ~ 1ms to probe masses $\gtrsim 10 \, M_\odot$. A distribution of the MVTs of Fermi/GBM GRBs inferred from the data using a wavelet analysis can be found in Ref. [31]. Apparently, variability of a few milliseconds is not uncommon, and GRBs with suitable MVT can be used to construct a valid dataset.

VI. CONCLUSIONS

In this paper we have investigated the use of GRBs to seek evidence of MACHO dark matter in the mass range $M_L \gtrsim 10 \, M_\odot$ via strong gravitational lensing. We have shown that performing an autocorrelation test for $\mathcal{O}(1000)$ GRBs with appropriate minimum variability timescales and background noise amplitudes can potentially result in sensitivity to $f_{\text{DM}} \sim 1\%$. This sensitivity in the mass range $10 - 100 \, M_\odot$ of interest requires GRBs with MVT ~ 1 ms.

The strength of the limits on f_{DM} depends on $\overline{R}$, the maximum detectable magnification (see Fig. 1). Fermi/GBM or Swift/BAT, however, are not capable of doing so. To achieve the level of $\overline{R}$ mentioned in Fig. 1, we would need a signal-to-noise power ratio of $r \sim 5000$. The distributions of power ratios for these two observatories are centered at $r \sim 10$ (with BAT improving on GBM by a factor ~ 3). In order for a future GRB observatory to fulfill the constraining potential of $f_{\text{DM}} \lesssim 1\%$, the noise amplitude (i.e. photon count) would have to be decreased further by an order of mangitude. This can potentially be done with improved localization accuracy.

Appendix A: Comparison between Fermi/GBM and Swift/BAT

One major difference between Fermi/GBM and Swift/BAT is that BAT uses a coded-aperture mask, which gives it a better imaging (i.e. localization) ability than GBM. This advantage is especially useful at lower photon energies: the CXB is stronger at lower energy, so BAT will significantly reduce more noise photons than GBM due to the coded-aperture mask. A comparison in Fig. 8 shows that from GBM to BAT there is an improvement of power ratio r from ~ 5 to ~ 7. Unfortunately, this is still not enough for our purpose.
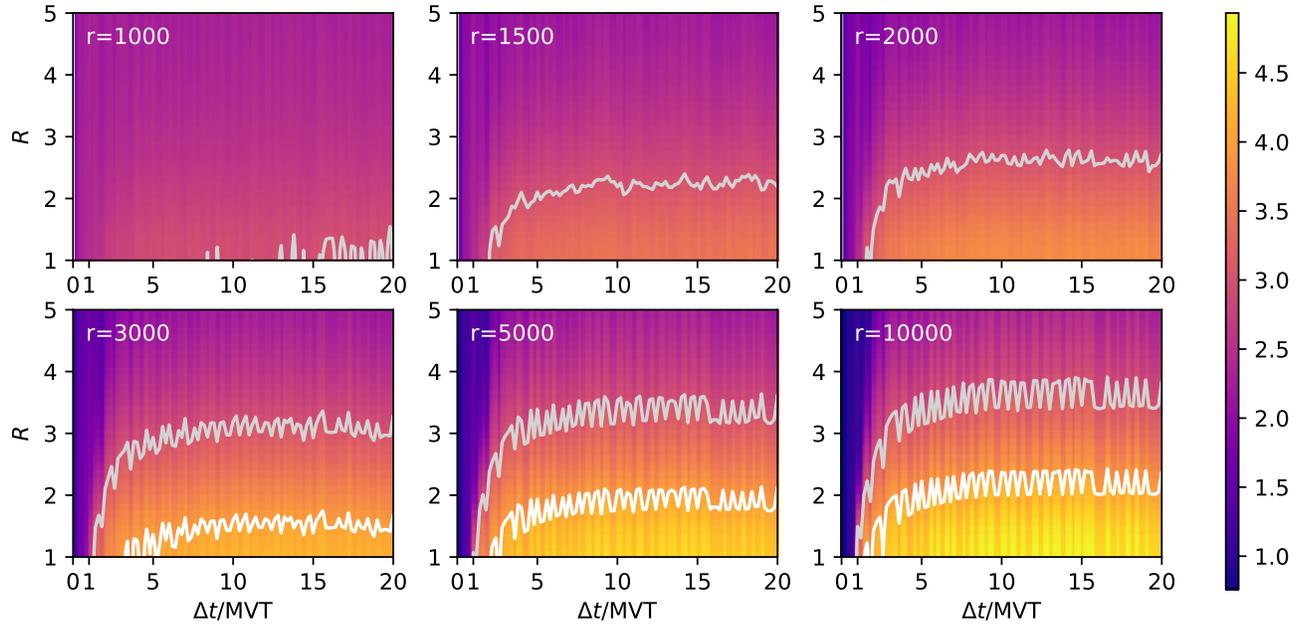
FIG. 7. Detection significance (in sigmas) for different time delays Δt and magnification ratios R in a simulated lensing experiment. We set MVT = 1 ms and use the MVT as the time delay unit. Gray (white) lines represent a 3σ (4σ) threshold. It can be seen that a higher signal strength r yields a better detection threshold $\overline{R}$, as expected. The plot shows that $r \sim 5000$ will result in a 3σ (4σ) detection at $\overline{R} = 3.0$ (2.0). Also, with this r, all time delays longer than $\overline{\Delta t} = $ MVT are detectable.

[1] G. Bertone, D. Hooper and J. Silk, "Particle dark matter: Evidence, candidates and constraints," Phys. Rept. **405**, 279 (2005) [hep-ph/0404175].

[2] R. A. Allsman *et al.* [Macho Collaboration], "MACHO project limits on black hole dark matter in the 1-30 solar mass range," Astrophys. J. **550**, L169 (2001) [astro-ph/0011506].

[3] P. Tisserand *et al.* [EROS-2 Collaboration], "Limits on the Macho Content of the Galactic Halo from the EROS-2 Survey of the Magellanic Clouds," Astron. Astrophys. **469**, 387 (2007) [astro-ph/0607207].

[4] L. Wyrzykowski *et al.*, "The OGLE View of Microlensing towards the Magellanic Clouds. IV. OGLE-III SMC Data and Final Conclusions on MACHOs," Mon. Not. Roy. Astron. Soc. **416**, 2949 (2011) [arXiv:1106.2925 [astro-ph.GA]].

[5] D. P. Quinn, M. I. Wilkinson, M. J. Irwin, J. Marshall, A. Koch and V. Belokurov, "On the Reported Death of the MACHO Era," Mon. Not. Roy. Astron. Soc. **396**, 11 (2009) [arXiv:0903.1644 [astro-ph.GA]].

[6] J. Yoo, J. Chaname and A. Gould, "The end of the MACHO era: limits on halo dark matter from stellar halo wide binaries," Astrophys. J. **601**, 311 (2004) [astro-ph/0307437].

[7] M. A. Monroy-Rodrguez and C. Allen, "The end of the MACHO era- revisited: new limits on MACHO masses from halo wide binaries," Astrophys. J. **790**, no. 2, 159 (2014) [arXiv:1406.5169 [astro-ph.GA]].

[8] T. D. Brandt, "Constraints on MACHO Dark Matter from Compact Stellar Systems in Ultra-Faint Dwarf Galaxies," Astrophys. J. **824**, no. 2, L31 (2016) [arXiv:1605.03665 [astro-ph.GA]].

[9] Y. Ali-Haïmoud and M. Kamionkowski, "Cosmic microwave background limits on accreting primordial black holes," Phys. Rev. D **95**, no. 4, 043534 (2017) [arXiv:1612.05644 [astro-ph.CO]].

[10] B. Horowitz, "Revisiting Primordial Black Holes Constraints from Ionization History," arXiv:1612.07264 [astro-ph.CO].

[11] D. Aloni, K. Blum and R. Flauger, "Cosmic microwave background constraints on primordial black hole dark matter," JCAP **1705**, no. 05, 017 (2017) doi:10.1088/1475-7516/2017/05/017 [arXiv:1612.06811 [astro-ph.CO]].

[12] M. Ricotti, J. P. Ostriker and K. J. Mack, "Effect of Primordial Black Holes on the Cosmic Microwave Background and Cosmological Parameter Estimates," Astrophys. J. **680**, 829 (2008) doi:10.1086/587831 [arXiv:0709.0524 [astro-ph]].

[13] B. P. Abbott *et al.* [LIGO Scientific and Virgo Collaborations], "Observation of Gravitational Waves from a Binary Black Hole Merger," Phys. Rev. Lett. **116**, no. 6, 061102 (2016) [arXiv:1602.03837 [gr-qc]].

[14] Y. B. Zeldovich and I. D. Novikov, Astronomicheskii Zhurnal **43**, 758 (1966).

[15] S. Hawking, Mon. Not. Roy. Astron. Soc. , **152**, 75 (1971).

[16] S. Bird, I. Cholis, J. B. Muñoz, Y. Ali-Haïmoud, M. Kamionkowski, E. D. Kovetz, A. Raccanelli and A. G. Riess, "Did LIGO detect dark matter?," Phys.

Rev. Lett. **116**, no. 20, 201301 (2016) [arXiv:1603.00464 [astro-ph.CO]].

[17] S. Clesse and J. Garca-Bellido, "The clustering of massive Primordial Black Holes as Dark Matter: measuring their mass distribution with Advanced LIGO," Phys. Dark Univ. **15**, 142 (2017) [arXiv:1603.05234 [astro-ph.CO]].

[18] M. Sasaki, T. Suyama, T. Tanaka and S. Yokoyama, "Primordial Black Hole Scenario for the Gravitational-Wave Event GW150914," Phys. Rev. Lett. **117**, no. 6, 061101 (2016) [arXiv:1603.08338 [astro-ph.CO]].

[19] A. Kashlinsky, "LIGO gravitational wave detection, primordial black holes and the near-IR cosmic infrared background anisotropies," Astrophys. J. **823**, no. 2, L25 (2016) doi:10.3847/2041-8205/823/2/L25 [arXiv:1605.04023 [astro-ph.CO]].

[20] M. Sasaki, T. Suyama, T. Tanaka and S. Yokoyama, "Primordial black holes: perspectives in gravitational wave astronomy," Class. Quant. Grav. **35**, no. 6, 063001 (2018) [arXiv:1801.05235 [astro-ph.CO]].

[21] E. D. Kovetz, "Probing Primordial-Black-Hole Dark Matter with Gravitational Waves," Phys. Rev. Lett. **119**, no. 13, 131301 (2017) [arXiv:1705.09182 [astro-ph.CO]].

[22] P. Meszaros, "Gamma-Ray Bursts," Rept. Prog. Phys. **69**, 2259 (2006) [astro-ph/0605208].

[23] A. Pe'er, "Physics of Gamma-Ray Bursts Prompt Emission," Adv. Astron. **2015**, 907321 (2015) [arXiv:1504.02626 [astro-ph.HE]].

[24] N. Gehrels and P. Meszaros, "Gamma Ray Bursts," Science **337**, 932 (2012) [arXiv:1208.6522 [astro-ph.HE]].

[25] C. S. Kochanek, "The Saas Fee Lectures on strong gravitational lensing," astro-ph/0407232.

[26] A. O. Petters, H. Levine, and J. Wambsganss, "Singularity Theory and Gravitational Lensing", Birkhuser, Boston, 2001.

[27] C. Meegan *et al.*, "The Fermi Gamma-Ray Burst Monitor," Astrophys. J. **702**, 791 (2009) [arXiv:0908.0450 [astro-ph.IM]].

[28] N. Gehrels *et al.* [Swift Science Collaboration], "The Swift Gamma-Ray Burst Mission," Astrophys. J. **611**, 1005 (2004) [astro-ph/0405233].

[29] W. S. Paciesas, Baltic Astronomy **13**, 187-192 (2004)

[30] J. B. Muñoz, E. D. Kovetz, L. Dai and M. Kamionkowski, "Lensing of Fast Radio Bursts as a Probe of Compact Dark Matter," Phys. Rev. Lett. **117**, no. 9, 091301 (2016) [arXiv:1605.00008 [astro-ph.CO]].

[31] G. A. MacLachlan *et al.*, "Minimum Variability Time Scales of Long and Short GRBs," Mon. Not. Roy. Astron. Soc. **432**, 857 (2013) [arXiv:1201.4431 [astro-ph.HE]].

[32] S. Mao, Gravitational microlensing of gamma-ray bursts, Astrophys. J. **402**, 382 (1993).

[33] J. M. Quashnock and D. Q. Lamb, "Evidence that gamma-ray burst sources repeat," Mon. Not. Roy. Astron. Soc. **265**, L59 (1993) [astro-ph/9307014].

[34] M. Tegmark, D. Hartmann, M. Briggs, J. Hakkila and C. Meegan, "Improved limits on gamma-ray burst repeti-

tion," Astrophys. J. **466**, 757 (1996) [astro-ph/9511079].

[35] J. Hakkila, C. A. Meegan, G. N. Pendleton, M. S. Briggs, J. M. Horack, D. H. Hartmann and V. Connaughton, "GRB repetition limits from current BATSE observations," AIP Conf. Proc. **428**, no. 1, 236 (1998) [astro-ph/9712092].

[36] J. Gorosabel, A. J. Castro-Tirado, S. Brandt and N. Lund, "A BATSE based search for repeaters in the sample of gamma-ray bursts detected by the WATCH experiment," Astron. Astrophys. **336**, 57 (1998) [astro-ph/9804239].

[37] R. J. Nemiroff, W. A. D. T. Wickramasinghe, J. P. Norris, C. Kouveliotou, G. J. Fishman, C. A. Meegan, W. S. Paciesas and J. M. Horack, "Null result in gamma-ray burst lensed echo search," Astrophys. J. **432**, 478 (1994) [astro-ph/9403045].

[38] O. S. Ougolnikov, "The search for possible mesolensing of cosmic gamma-ray bursts. double and triple bursts in batse catalogue," astro-ph/0111215.

[39] R. J. Nemiroff, G. F. Marani, J. P. Norris and J. T. Bonnell, "Limits on the cosmological abundance of supermassive compact objects from a millilensing search in gamma-ray burst data," Phys. Rev. Lett. **86**, 580 (2001) [astro-ph/0101488].

[40] P. Veres, Z. Bagoly, I. Horvath, A. Meszaros and L. G. Balazs, "A search for gravitational lensing effects in Fermi GRB data," arXiv:0912.3928 [astro-ph.CO].

[41] Y. Hirose, M. Umemura, A. Yonehara and J. Sato, "Imprint of Gravitational Lensing by Population III Stars in Gamma Ray Burst Light Curves," Astrophys. J. **650**, 252 (2006) [astro-ph/0605548].

[42] D. W. Hogg, "Distance measures in cosmology," astro-ph/9905116.

[43] D. Coward, E. Howell, M. Branchesi, G. Strata, D. Guetta, B. Gendre and D. Macpherson, "The Swift Gamma-Ray Burst redshift distribution: selection biases and optical brightness evolution at high-z?," Mon. Not. Roy. Astron. Soc. **432**, 2141 (2013) [arXiv:1210.2488 [astro-ph.CO]].

[44] D. Gruber *et al.*, "The Fermi GBM Gamma-Ray Burst Spectral Catalog: Four Years Of Data," Astrophys. J. Suppl. **211**, 12 (2014) [arXiv:1401.5069 [astro-ph.HE]].

[45] R. N. Bracewell, "The Fourier transform and its applications", Vol. 31999, McGraw-Hill, New York, 1986.

[46] B. B. Mandelbrot and J. W. Van Ness, "Fractional brownian motions, fractional noises and applications", SIAM Review **10**, 422-437 (1968).

[47] P. Flandrin, "On the spectrum of fractional brownian motions", IEEE Transactions on Information Theory **35**, 197-199 (1989).

[48] M. Ajello *et al.*, "Cosmic X-ray background and Earth albedo Spectra with Swift/BAT," Astrophys. J. **689**, 666 (2008) [arXiv:0808.3377 [astro-ph]].
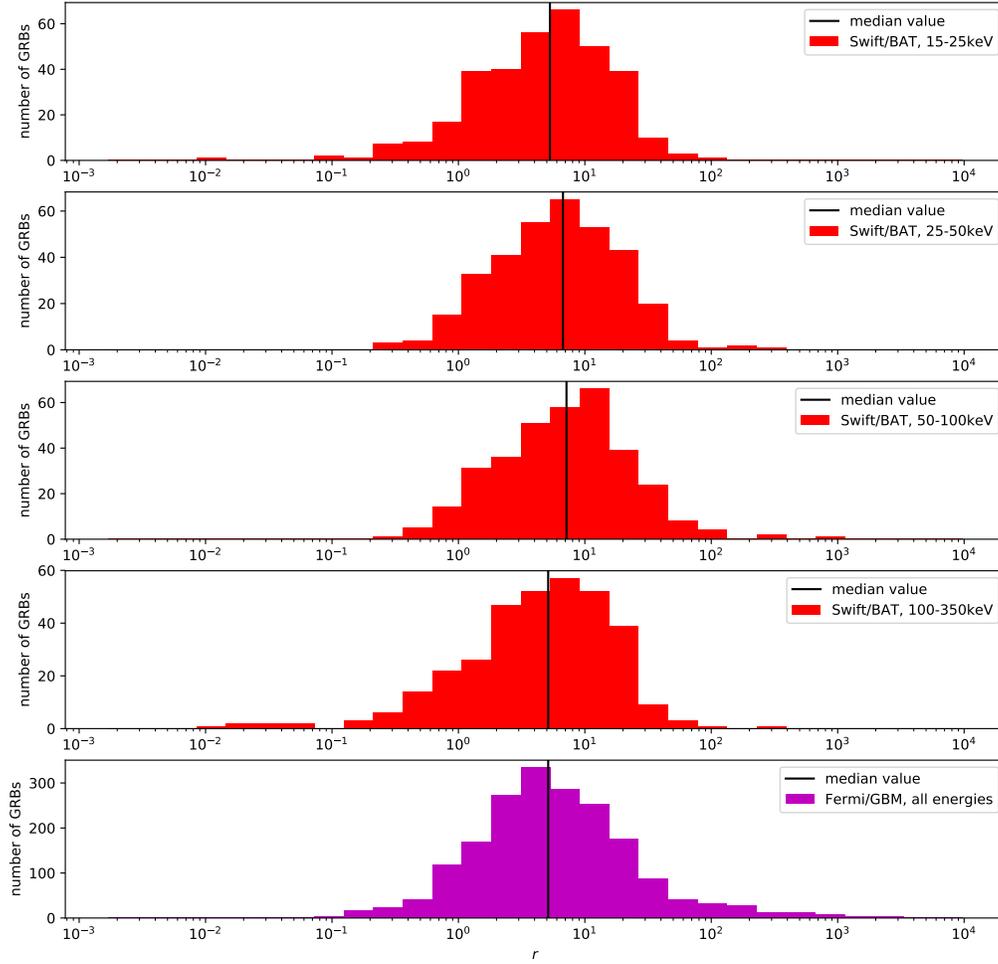
FIG. 8. Power ratio r distribution in Fermi/GBM and Swift/BAT, with BAT power ratio shown for each energy bin. Black vertical lines are the median values of each distribution. In the relevant energy bins ($E < 100$keV), from GBM to BAT there is an improvement of power ratio r from ~ 5 to ~ 7.